ELSEVIER

Coordination Chemistry Reviews
190–192 (1999) 1101–1123

COORDINATION CHEMISTRY REVIEWS

www.elsevier.com/locate/ccr

X-ray absorption spectroscopy in coordination chemistry

James E. Penner-Hahn [a,b,*]

[a] *Section de Bioénergétique, CNRS URA 2096, DBCM, CEA Saclay, F-91191 Gif-sur-Yvette Cedex, France*
[b] *Department of Chemistry, The University of Michigan, 930 N. University Avenue, Ann Arbor, MI 48109-1055, USA*

Contents

* Correspondence address: Department of Chemistry, The University of Michigan. Fax: + 1-734-647-4865.
E-mail address: jeph@umich.edu (J.E. Penner-Hahn)

PII: S0010-8545(99)00160-5

Abstract

X-ray absorption spectroscopy (XAS) is one of the premier tools for investigating the local structural environment of metal ions. XAS can be divided into X-ray absorption near edge structure (XANES), which provides information primarily about geometry and oxidation state, and extended X-ray absorption fine structure (EXAFS) which provides information about metal site ligation. One of the key attractions of XAS is that it can be used regardless of the physical form of the sample, and in particular it can be used to study non-crystalline materials. Consequently, XAS has come to be widely utilized by the biochemistry and materials science communities. Recently, however, it has become clear that there are numerous questions of interest to coordination chemists that can be addressed using XAS. In this contribution, the physical basis of XAS is reviewed, the advantages and limitations of the technique are discussed, and several examples of the applications of XAS to coordination chemistry are presented. The prospects for future applications of XAS are summarized.

Keywords: X-ray absorption spectroscopy; Coordination chemistry; Structural environment

1. Introduction

Structural characterization of metal complexes has played a crucial role in the development of coordination chemistry. Despite the tremendous advances that have taken place in spectroscopic methods for structure elucidation, X-ray crystallography remains the method of choice for definitive determination of the structure of a new coordination complex.

Unfortunately, X-ray crystallography cannot always be used. Some samples simply cannot be crystallized in diffraction quality crystals, despite the best efforts of skilled experimenters. In other cases, crystals may be available but the structural questions of interest involve solution structure. For example, it may be necessary to determine whether a molecule remains structurally intact in solution. Finally, there are a variety of situations, involving for example crystallographic disorder, in which X-ray crystallography is unable to provide a complete structural description. In all of these cases, X-ray absorption spectroscopy (XAS) can provide unique structural information.

XAS has been known for most of this century, and has been available as a useful structural probe for over 25 years. Much of the interest in XAS, however, has focused on its applications to biological systems and to amorphous materials [1–5]. These were natural areas for early developments of XAS, since in both areas, almost all of the samples of interest are non-crystalline. In this context, any structural information is valuable.

In contrast, XAS has found fewer applications in coordination chemistry, perhaps because X-ray crystallography is such a powerful tool for the structural characterization of coordination complexes. The goal of this tutorial article is to review the physical principles of XAS and to illustrate through selected examples

why XAS should be thought of as a key tool in the toolkit of the coordination chemist. A variety of excellent reviews of X-ray absorption have been written, as have several monographs. It is not the intent of this review to repeat this information; the interested reader should consult one of these sources for a more detailed description of X-ray absorption [1–8]. Rather, it is the intent of this review to provide sufficient background information that the potential of X-ray absorption for solving problems in coordination chemistry will be clear.

2. The physical basis of X-ray absorption

X-ray energies are sufficiently high to eject, via the photoelectric effect, one or more core electrons from an atom. Each core electron has a well-defined binding energy, and when the energy of the incident X-ray is scanned across one of these energies, there is an abrupt increase in the absorption coefficient. This is the so-called 'absorption edge' of the element. Absorption edges are named according to the electron that is excited (K = 1s; L_I = 2s; L_{II}, L_{III} = 2p, etc.). There are two L edges for the 2p initial state due to spin-orbit coupling, which splits the $2p_{1/2}$ and $2p_{3/2}$ final states.

The importance of XAS derives from the fact that there is fine structure superimposed on the absorption edge. This fine structure is often divided into extended X-ray absorption fine structure (EXAFS), referring to structure well above the absorption edge, and X-ray absorption near edge structure (XANES), for structure in the immediate vicinity of the edge (see Fig. 1). The physical basis of both EXAFS and XANES is the scattering of the X-ray excited photoelectron by

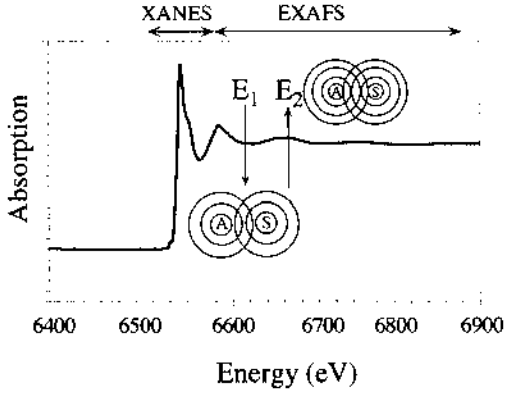

Fig. 1. Schematic illustration of an X-ray absorption spectrum at the Mn K edge. The insets show the interference phenomena that give rise to the modulations in absorption cross-section (see text). In the inset, **A** and **S** refer to the absorbing and scattering atoms, respectively. The concentric circles around **A** and **S** represent the maxima in the photoelectron wave that describes the propagation of the X-ray excited photoelectron. The $1s \rightarrow 3d$ transition is the very small peak at ca. 6550 eV, before the rising edge.

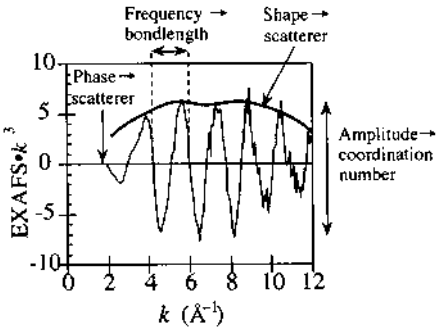

Fig. 2. Schematic illustration of the information content of an EXAFS spectrum. Qualitatively, the available information is the amplitude, the frequency, and the phase of the EXAFS oscillations. To a first approximation, amplitude is proportional to coordination number, while frequency is inversely related to bond length (i.e. for longer distances, there are more ways to have constructive or destructive interference). The phase of the EXAFS and the shape of the amplitude envelope provide information about scatterer type.

the surrounding atoms, and thus, the distinction between the regions is somewhat arbitrary. The acronym XAFS (X-ray absorption fine structure) has gained some currency as a reference to the entire structured absorption region (XANES + EXAFS).

2.1. EXAFS oscillations

The photoexcitation cross-section is modulated by the interference between the out-going and the back-scattered photoelectron waves. This is illustrated schematically in the insets to Fig. 1. As the X-ray energy increases, the kinetic energy of the photoelectron (i.e. the excess energy above the binding threshold) increases. This results in a decreasing photoelectron wavelength, and thus, in alternating destructive interference (energy E_1 in Fig. 1) and constructive interference (energy E_2 in Fig. 1). The physical origin of EXAFS is thus electron scattering, and EXAFS is best thought of as a spectroscopically-detected scattering method, rather than as a more conventional spectroscopy.

For a single absorber–scatterer pair (e.g. for a diatomic gas) this alternating interference will give rise to sinusoidal oscillations in the absorption coefficient if the energy is given in units proportional to the inverse photoelectron wavelength (the photoelectron wavevector, or k, defined as in Eq. (1)). In Eq. (1), the threshold energy, E_o, is the binding energy of the photoelectron.

$$k = \sqrt{2m_e(E - E_o)/\hbar^2} \tag{1}$$

In XAS analyses, it is typical to define the EXAFS, $\chi(k)$, as the fractional modulation in the X-ray absorption coefficient. The observed oscillations then

have an appearance similar to that shown in Fig. 2, and can then be described by an equation similar to Eq. (2).

$$\chi(k) = \sum_{s} \frac{N_s A_s(k) S_0^2}{kR_{as}^2} \exp(-2R_{as}/\lambda(k)) \exp(-2k^2\sigma_{as}^2) \cdot \sin(2kR_{as} + \phi_{as}(k)) \qquad (2)$$

In Eq. (2), the parameters that are of principal interest to the coordination chemist are the number of scattering atoms, N_s and the absorber–scatterer distance, R_{as}. To a first approximation, these can be related to the depth of modulation (i.e. the EXAFS amplitude) and the frequency of the modulations, respectively, as shown in Fig. 2. There are, however, a variety of other parameters that must either be determined or be defined in order to extract the chemically relevant information. Chief among these are $A_s(k)$ and $\phi_{as}(k)$. These represent, respectively, the energy dependence of the photoelectron scattering, and the phase shift that the photoelectron wave undergoes when passing through the potential of the absorbing and scattering atoms. These amplitude and phase parameters contain the information necessary to identify the scattering atom. Thus, for example, sulfur and oxygen introduce phase shifts, $\phi_{as}(k)$, that differ by approximately π. Unfortunately, both $A_s(k)$ and $\phi_{as}(k)$ depend only weakly on scatterer identity, and thus, it is difficult to identify the scatterer with precision. For the coordination chemist, this typically means that O and N, or S and Cl cannot be distinguished, while O and S can. Of course, scatterers such as C and F also cannot be distinguished. However, in practice this ambiguity seldom causes problems, since the chemical identity of the sample is (presumably) known.

The EXAFS amplitude falls off as $1/R^2$. This reflects the decrease in photoelectron amplitude per unit area as one moves further from the photoelectron source (i.e. the absorbing atom). The main consequence of this damping is that the EXAFS information is limited to atoms in the near vicinity, typically within 10 Å of the absorber. There are three additional damping terms in Eq. (2). The S_0^2 term is introduced to allow for inelastic loss processes and is typically not refined in EXAFS analyses. The first exponential term is a damping factor that arises from the mean free path of the photoelectron ($\lambda(k)$). This serves to limit further the distance range that can be sampled by EXAFS. The second exponential term is the so-called 'Debye–Waller' factor. This damping reflects the fact that if there is more than one absorber–scatterer distance, each distance will contribute EXAFS oscillations of a slightly different frequency. The destructive interference between these different frequencies leads to damping in the EXAFS amplitude. The Debye–Waller factor, σ_{as}, is the root-mean-square deviation in absorber–scatterer distance. This damping is always present due to zero-point thermal motion, and may, for polyatomic systems, also occur as a consequence of structural disorder.

The summation in Eq. (2) reflects the fact that all absorber–scatterer pairs contribute to the observed oscillations. In practice, however, it is not realistic to refine all of the different absorber–scatterer interactions. Consequently it is necessary to group absorber–scatterer interactions into 'shells'. A shell is a group of similar scatterers at approximately the same distance from the absorber.

2.2. Fourier transformation

Although Eq. (2) provides a complete description of the EXAFS oscillations, it is not a particularly convenient form for visualizing the information content of an EXAFS spectrum. As with NMR spectroscopy, Fourier transformation can be used to decompose a frequency-space signal into its different constituent frequencies. This is illustrated for a CuCN solution in Fig. 3. For EXAFS, the canonical variables are k (in Å^{-1}) and R (in Å), and the Fourier transform (FT) of an EXAFS spectrum gives a pseudo-radial distribution function. It is pseudo in that the FT amplitude cannot be related directly to electron density around the absorber due to the $A_s(k)$ factor and the damping factors in Eq. (2), and because the apparent distances in the FT are shifted by about -0.5 Å due to the phase shift $\phi_{as}(k)$. The FT is a useful way of judging qualitatively what shells may be present in a system and for comparing a fit to the data. However, it is important to remember that Fourier transforms are subject to several potential artefacts. In many cases, multiple shells of scatterers do not give rise to multiple peaks in the FT [8]. Similarly, interference between two different peaks in the FT may give rise to a spurious third peak. The latter results from the fact that the FT of an EXAFS spectrum is actually a complex number, with both real and imaginary components. Typically, however, only the modulus of the FT is plotted. This is useful for visualizing the major contributions to the EXAFS spectrum, but should never be used for quantitative data analysis.

2.3. Curve fitting

Quantitative analysis of EXAFS spectra typically involves using an equation similar to Eq. (2) to model the observed oscillations. The fitting can be done either in k space or in R (Fourier transform) space, with essentially equivalent results. The parameters that define the scattering ($A_s(k)$, S_0^2, $\phi_{as}(k)$, and $\lambda(k)$) are determined either from ab initio calculations or from model compounds of known structure. In recent years, the available theoretical methods for quickly and accurately calculating these parameters have improved dramatically. Ab initio calculations are now relatively straightforward [9–11], although careful comparison with model compounds remains important for proper calibration of the calculated parameters [12]. Once these parameters have been specified, the structurally related parameters (N_s, $\sigma_{as}(k)$, and R_{as}) are refined, usually via a non-linear least-squares fitting procedure.

2.4. XANES structure

The physical principles that govern EXAFS apply equally in the XANES region. However, at low kinetic energy the photoelectron mean-free-path increases dramatically. Similarly, the $\exp(-k^2)$ dependence of the Debye–Waller factor means that this damping factor is negligible in the XANES region. These effects combine to render the XANES region sensitive to a wide range of absorber–scatterer distances, as compared to the (relatively) simple short-range treatment that can be used for

most EXAFS. This is, in principle, an advantage since it provides the possibility of extracting three-dimensional structure information from XANES spectra (see discussion of multiple scattering below). However, this also makes theoretical simulations of XANES spectra extremely difficult. Although much progress has recently

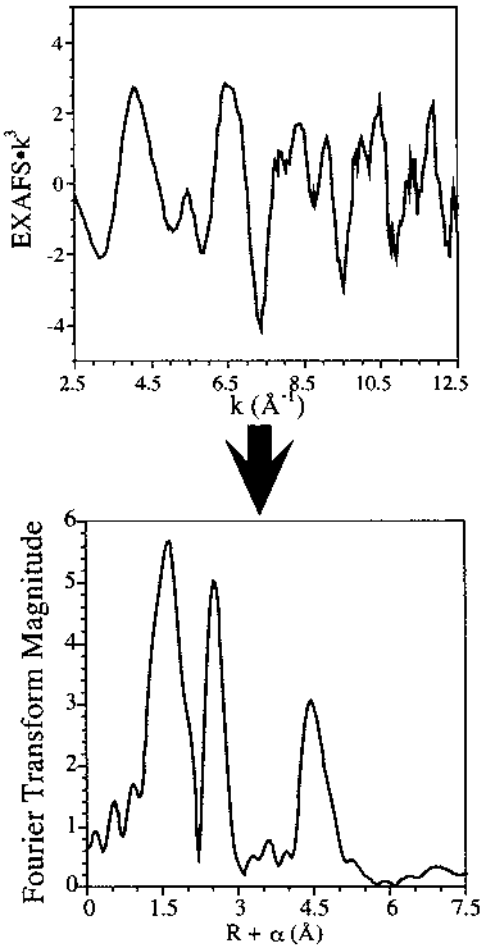

Fig. 3. Illustration of relationship between k-space and R-space information in EXAFS. Top spectrum is the EXAFS data for a solution of CuCN·2LiCl in THF. The oscillations are weighted by k^3 to enhance the magnitude at high k. The lower figure is the modulus of the Fourier transform of these data, showing the pseudo-radial distribution function around the Cu. For clarity, the real and imaginary components of the Fourier transform are not shown. The two plots are necessarily equivalent, since Fourier transformation cannot change the information content of the data. In the R-space presentation, the presence of three main shells of scattering atoms is clear; evidence for multiple scatterers can also be seen in the pronounced beats in the k-space presentation. The three main peaks at $R+\alpha \approx 1.6$, 2.5, and 4.5 Å correspond to Cu–C nearest neighbors at ca. 1.9 Å, Cu···N next-nearest neighbors at ca. 3 Å and Cu···Cu next-next-nearest neighbors at ca. 5 Å. The peaks are shifted from the true distance by the EXAFS phase shift. See text and Fig. 6 for discussion of the interpretation of these data.

been made in the theoretical modeling of XANES, most of the applications of this energy region remain qualitative. Nevertheless, the ability to make fingerprint-like comparisons of XANES spectra can be important in identifying an unknown structure.

On the low energy side of the absorption edge one frequently observes several weak transitions. In contrast with the electron-scattering model that is used to describe the EXAFS and the other XANES features, these low energy transitions arise from bound state transitions. For the first transition series metals, bound state transitions include both $1s \rightarrow 3d$ and $1s \rightarrow 4p$ transitions. An exciting recent development in XAS has been the development of theoretical models that can use the bound-state transitions to extract information about the electronic structure of the absorbing atom (see below).

2.5. Advantages of XAS

The principal advantage of XAS as a structural probe is that it is a local structure probe. None of the discussion above requires the presence of long-range order. This means that XAS can be used to study non-crystalline samples or to compare solution structure with solid state structure. In ideal circumstances (see below for some of the limitations), EXAFS data can be analyzed to determine the absorber–scatterer distance with an accuracy of ca. 0.02 Å and a precision that is substantially better (0.004 Å [13], and perhaps even better under carefully controlled conditions). Coordination numbers can be determined with an accuracy of ca. 25% and scatterer identity can typically be defined to the nearest row of the periodic table.

In comparison with small molecule crystallography, the information available from XAS is relatively limited. However, for non-crystalline systems, XAS may provide the only available structural information. Even for crystalline systems, there are cases in which EXAFS can provide a different, and perhaps better, structural description than is available from crystallography. Several examples of this are discussed below. Finally, XAS has, through XANES transitions, the ability to provide oxidation state and spin-state information that can be difficult or impossible to extract from crystallographic measurements.

In comparison with other spectroscopic methods, XAS has the decided advantage that it is always detectable, without the need for specific spin states or isotopic substitution, and that it is element specific. Every element has at least one unique absorption edge, although for the very light elements, this edge energy may actually be in the UV, not in the X-ray region. For elements heavier than about phosphorous, measurement of the X-ray absorption spectrum is relatively straightforward using modern synchrotron X-ray sources, and even the lighter elements are studied frequently. The universal detectability of XAS is, of course, a mixed blessing since it means that XAS is a bulk technique sensitive to all of the forms of an element that are present in a sample. If the element of interest occurs in multiple environments only the average structure can be determined.

2.6. Limitations of XAS

Any discussion of the advantages of XAS would be incomplete without a summary of the limitations of the technique. Ultimately, all of these involve different limitations in experimental resolution. Several of these are widely recognized. As noted above, EXAFS provides only limited chemical resolution—scattering atoms that differ by two or three in atomic number (e.g. C, O, N, and F) typically cannot be resolved. EXAFS, at least as described thus far, provides no angular resolution. It is thus not possible to learn anything directly about geometry. There are some possibilities for introducing angular resolution (see below) but this remains a limitation in most XAS studies. Finally, the finite k range of the EXAFS spectrum limits the bond-length resolution of the method. Two scattering shells can only be resolved if they differ sufficiently in frequency to cause a detectable change in the EXAFS amplitude, due to the interference between the two different EXAFS components. For small differences in distance, the interference simply introduces an exponential damping factor. This is indistinguishable from an increase in the Debye–Waller term in Eq. (2). For perfect data, two shells of the same scatterer should become resolvable when the difference in their distances, δR, is large enough to cause a 'beat' in the EXAFS amplitude. This occurs for

$$\delta R \geq \pi/2k_{\max} \tag{3}$$

where $k_{\max}$ is the maximum value of k for which a signal can be measured. Typical values of $k_{\max}$ range from 12 to 20 Å^{-1}, depending on the composition and the concentration of the sample, giving $\delta R \approx 0.08$–0.13 Å. In reality, Eq. (3) gives a somewhat optimistic estimate of the minimum resolvable distance, since it assumes noise free data at $k_{\max}$. In practice, $k_{\max}$ is often defined as the point at which the noise level of the data becomes too large to permit reliable analysis. This is illustrated, for example, in Fig. 4 of Ref. [8].

2.7. Information content of EXAFS spectra

There is one additional limitation to EXAFS that is not as widely appreciated. Like all spectra, EXAFS spectra contain only a finite amount of information. In the case of EXAFS this information content is easily quantified. If δR in Eq. (3) gives the minimum separation that can be detected, and if the useful data covers an R range of ΔR, then the number of independent data points is given simply by $\Delta R/\delta R$. Since the useful k range does not extend to $k = 0$ Å^{-1}, a better expression for the number of independent data points, N_{idp}, is

$$N_{\text{idp}} = 2\Delta k\ \Delta R/\pi \tag{4}$$

Using Eq. (4) with typical values of $\Delta R = 2$ Å (e.g. useful information for $R = 1$–3 Å) and $\Delta k = 12$ Å^{-1} ($k = 2$–14 Å^{-1}), there are approximately 16 degrees of freedom in a typical data set. More involved derivations give slightly different N_{idp} values [14], but do not alter the essential result that the number of available degrees of freedom is severely limited. If one used crystallographic criteria that the

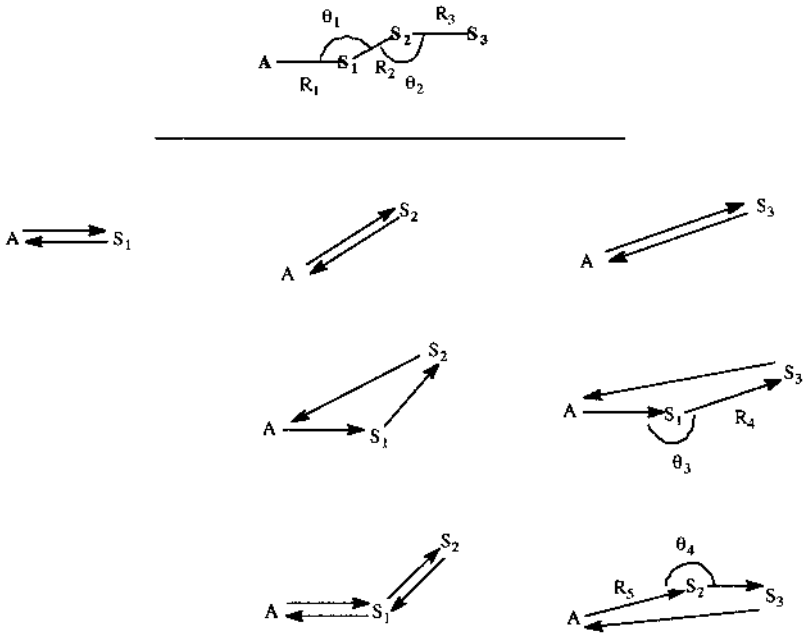

Fig. 4. Selected single and multiple scattering pathways for a tetraatomic system. (Top) Geometry of the absorber (A) relative to the three scattering atoms. The positions can be specified by three distances and two angles (for a planar system). (Bottom) Scattering pathways for outgoing and backscattered photoelectron (indicated by arrows). Left column is for the nearest neighbor, S_1; Middle for S_2; and Right for S_3. For S_1, only the single scattering pathway is shown. For S_2, both double and triple scattering pathways are also indicated. For S_3, only two of the possible double scattering pathways are shown. Note that, for a non-planar system, several additional distances and angles are required to completely specify the scattering pathways. In general, all possible multiple scattering pathways (of which only a small fraction are shown) will contribute to the observed EXAFS, each with oscillations of slightly different frequency.

minimum acceptable data/parameter ratio is 6–10, this would limit the typical EXAFS analysis to approximately two variable parameters. In reality, the situation is not quite this grim, but the fact remains that careful limitation of the number of variable parameters is necessary if one is to obtain reliable information from EXAFS [12,15].

Similar problems with parameter under-determination are well known in protein crystallography. In that case, the solution has been to include structural constraints, such as the known bond lengths and angles within amino acids, as part of the refinement. This approach has been used to good effect in refinements of the EXAFS scattering by rigid imidazole group as a ligand in bioinorganic complexes [11,16,17]. By adding constraints, it is possible to increase the number of shells that are used to describe the EXAFS without increasing (too much) the number of freely variable parameters. It is important to keep in mind, however, that constraints are only as good as the model upon which they are based. Erroneous assumptions in building the constraints may result in incorrect results in the fits.

For seriously under-determined systems, even constrained refinements may give a data:parameter ratio that is not much larger than 1 (or even smaller than 1 in some instances). In such cases, it is better to think of the EXAFS simulation (Eq. (2)) as showing that a particular structural model is consistent with the data, rather than showing that it is required by the data. Although genuine curve fitting and data simulation are both legitimate approaches to interpreting EXAFS spectra, it is important to remember that they do not provide the same information. Curve fitting, when done properly, describes the structural parameters that are required by the data. In contrast, a successful simulation gives only a model of the data, not necessarily the correct model.

It is important to note that Eq. (4) is a general property of EXAFS, and is not a specific consequence of Fourier filtering. Some authors have concluded that ΔR is effectively unlimited, or limited only by λ, so long as the data are not filtered. This is analogous to assuming that the information content of an NMR experiment can be doubled by sampling the FID at twice the frequency. The latter would only be true if the width (chemical shift range) of the NMR spectrum was such that the FID was under-sampled. In the case of EXAFS, ΔR (and thus the information content) is defined by the range of R space over which there is chemically useful information.

An analogous error is to confuse the number of measured data points, N_p, with the number of independent data points, N_{idp} in Eq. (4). A widely quoted statistical test uses N_p to calculate a χ^2 statistic which can be used with the F-test to determine whether an added shell is significant [18]. Since N_p is typically 10–15 times larger than N_{idp} (i.e. EXAFS data are typically over-sampled by a factor of 10–15), the use of N_p rather than N_{idp} in the F-test dramatically overestimates the significance of an added shell.

Statistical tests, with the correct N_{idp}, can be used to judge whether an added shell is required by the data [19,20]. However, several authors have noted [12,15] the need to exercise caution with these tests in order to avoid either false positives (inclusion of shells that are not actually present) or false negatives (exclusion of shells that are present).

There are several possibilities for obtaining additional information from XAS, thereby avoiding some of the limitations discussed in the preceding paragraphs. Perhaps the most important of these is the possibility of using multiple scattering to obtain information about the geometry of an absorbing atom.

2.8. Multiple scattering

In the physical model presented above, the X-ray excited photoelectron travels from the absorbing atom to the scattering atom and back. However, far more complex scattering pathways are also possible. For example (see Fig. 4), the photoelectron may travel from the first scattering atom (S_1) to a second (S_2) and even a third (S_3) before returning to the absorbing atom. Each scattering interaction defines an angle, e.g. θ_1 in Fig. 4, that determines the intensity, and hence the significance, of that multiple-scattering pathway. The scattering of an electron by

an atom is strongly focused in the forward direction ($\theta \approx 180°$) and falls off very rapidly for $\theta \lessapprox 150°$.

Multiple scattering depends on the simultaneous positions of three or more atoms, i.e. on the distances and angles between the atoms. This means that multiple scattering can, at least in principle, provide information about the three-dimensional structure around the absorbing site. For this reason, there has been a great deal of interest in developing methods to use multiple scattering in XAS analyses, and thus to avoid the limitation that EXAFS provides only radial structure information.

Unfortunately, the situation is not quite so promising as the previous paragraphs might suggest. Two obstacles confront attempts to use multiple-scattering to determine molecular geometry. The first is computational: since hundreds, and even thousands of multiple scattering pathways can contribute to the observed XAS, the theoretical description of multiple scattering can be computationally formidable. This makes it difficult to perform effective refinements of complete multiple scattering. However, this has become a less important issue as multiple-scattering programs have improved and as computational power has increased.

A more fundamental problem is the limited information content of XAS spectra (e.g. Eq. (4)). Multiple scattering is most important for outer-shell atoms beyond the first coordination sphere. In Eq. (4), the information content of XAS increases linearly as the R range of the data increases. Unfortunately, the number of possible scattering atoms increases approximately as R^2. It is thus apparent that at some point, the increase in information content is overwhelmed by the increase in variable parameters. This is illustrated schematically in Fig. 5. For an idealized, high symmetry system (**A** in Fig. 5), only three parameters are needed to completely describe the structure. In such a situation, it is quite feasible to analyze EXAFS data measured over any reasonable k range to determine the geometry (in this case, the angle of the coordinated cyanide). In a lower symmetry, but perhaps more realistic model (**B** in Fig. 5), the situation is much more complicated. The nearest neighbor M–N and M–O interactions may require as many as four distances for a complete description, although only one (R_1) is shown in Fig. 5. Depending on the structure, it may be appropriate to group these nearest neighbor distance into one or two average shells, each defined by a distance and a Debye–Waller factor; however, this still represents an increase in comparison to the one nearest-neighbor parameter required in **A**. The description of the second shell is even more complicated. The carboxylate carbon alone may require as many as four additional parameters (R_2, R_3, θ_1, and θ_2 in Fig. 5). A complete description of the multiple scattering for the second shell scattering for this hypothetical molecule could require as many as ten additional parameters, beyond the four used to describe the first shell.

Due to this mismatch between available information and required parameters it is usually necessary to simplify the geometry used to model a site (for example, to assume high symmetry). Providing these approximations are valid, multiple scatter-

ing can be used to provide detailed information about a metal site. An example of this is described below. However, it is important to keep in mind the possibility that the simplifying assumptions may not be valid, and may, as a consequence, introduce significant errors into the refined structural parameters.

3. Applications

Notwithstanding the dire warnings (above) regarding the limitations of XAS, the fact remains that XAS has the ability to provide unique information about coordination compounds. In the following, several examples of the application of XAS to coordination chemistry are discussed. There is no attempt to provide a comprehensive summary of all of the published applications. Rather, these are selected examples chosen to illustrate how XAS can be used to answer different classes of questions in coordination chemistry.

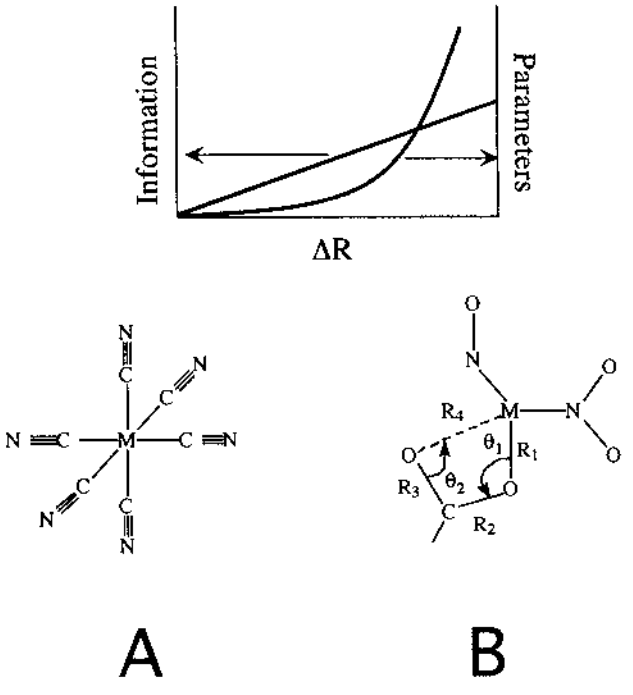

Fig. 5. (Top) Schematic illustration of the approximate relationship between information available and information required for analysis of data as a function of R range. (Bottom) Specific examples illustrating the graph above. **A** is a high symmetry molecule; **B** is a lower symmetry, but perhaps more realistic site. For **A**, detailed analysis of the multiple scattering is clearly possible; for **B**, the number of variables required for a complete analysis of the multiple scattering is likely to exceed the available information unless constraints of some kind can be introduced.

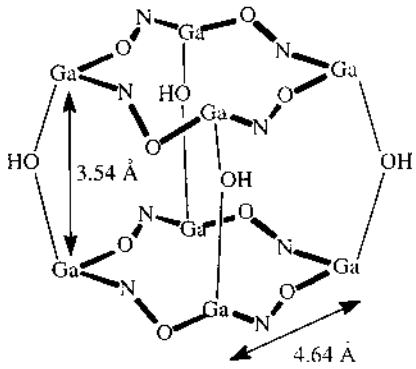

Fig. 6. Schematic illustration of the Ga 12-metallacrown-4 cryptate structure. Only the core atoms of the two metallacrown rings are shown. The EXAFS detectable 3.54 Å inter-ring Ga–Ga distance and the EXAFS non-detectable 4.64 Å intra-ring Ga–Ga distance are shown by the arrows.

3.1. Does a structure remain intact in solution?

Although X-ray crystallography is extremely powerful as a structural probe, it provides only a description of the structure in the solid state. In contrast, most chemical reactions take place in solution. If structure is to be used to understand reactivity, it is essential to confirm that the crystallographic structure accurately represents the molecule of interest when it is in solution. This is particularly important for multinuclear aggregates, which might be expected to dissociate into smaller units when dissolved. In such cases, XAS can be used as a fingerprint for comparing between solid state and solution structures. One example of such an application involves the solution structure of a Ga metallacrown complex synthesized by Pecoraro and co-workers [21]. Salicylhydroximate and Ga combine to form the inorganic analog of a 12-crown-4 crown ether, and the crystal structure of the sodium salt of this metallacrown showed clearly that it self-assembles with hydroxide to form an inorganic analog of a cryptate (shown schematically in Fig. 6). It was not clear, however, that this structure remained intact in solution. In this case, EXAFS was able to provide unambiguous evidence that the 3.54 Å Ga–Ga interactions between Ga ions in different rings remain intact in solution. This is diagnostic of the intact cryptate structure.

There are, of course, many other techniques that can be used to compare solid state and solution structure. These include Mössbauer, EPR, NMR, FTIR, and UV–vis spectroscopy. All of these, together with EXAFS, are limited by the necessity of assuming that the 'fingerprint' that is compared is a unique marker for the structure of interest. EXAFS would not be a particularly useful technique for determining whether a nitrogen base remains coordinated in solution or is displaced by a solvent molecule (assuming an *N*- or *O*-coordinating solvent). However, EXAFS is extremely useful for detecting metal–metal interactions and determining whether they remain intact in solution.

In the Ga example, the inter-ring Ga–Ga interaction (3.54 Å) was readily detectable. However, the longer 4.64 Å intra-ring Ga–Ga distance was not detectable in the EXAFS. In part, this reflects the greater detectability of shorter distances. In addition, the inter-ring Ga–Ga pair is bridged by a single atom (hydroxide) while the intra-ring galliums have a multi-atom bridge which apparently results in much greater variation in the Ga–Ga distance (the σ^2 factor in Eq. (2)). In general, single-atom bridges are much more likely than other bridging geometries to give detectable metal–metal interactions in EXAFS [8].

In the Ga example, EXAFS would not have been particularly useful for demonstrating that the 12-metallacrown-4 ring remained intact in solution, since the intra-ring Ga–Ga interaction is not readily detectable even in the solid state. In general, it is always important to remember that the absence of a signal in the EXAFS is not necessarily evidence for the absence of the interaction in the sample. If the interaction is weak enough (σ^2 large enough), even nearest neighbors can be non-detectable in EXAFS [22,23].

In some cases, XANES may be a more useful fingerprint than EXAFS for solute structure determination. For a series of bis(*N*-alkylsalicyladiminato)copper(II) complexes, the structural question was not ligation but geometry. From a variety of other spectroscopies, it was clear that the Cu(II) was approximately tetragonal, with O_2N_2 ligation, but it was not clear to what extent the Cu site distorted towards a tetrahedral structure as a function of changes in solvent [24]. There were no differences in Cu-ligand bond lengths as a function of solvent, but there were characteristic changes in the XANES region, particularly in the $1s \rightarrow 3d$ and $1s \rightarrow 4p$ regions, that could be interpreted in terms of geometric distortions.

A related application of EXAFS is to determine the solvation environment of metal cations in solution. This is superficially analogous to the comparison of solid and solution structure, but is in fact much more difficult. The structural question is, for example, whether or not a counter ion is coordinated. There have been several recent studies of Cu(II) coordination in aqueous solution [25,26]. These used an elaborate fitting procedure including a variety of multiple scattering interactions. The difficulty with this approach is that a reasonable description of the structural possibilities requires a very large number of variable parameters. For example, 27–29 variable parameters were needed to describe the data for Cu(II)–glycinate complexes in solution [25]. Since the useful EXAFS signal only extends to $R \leq \approx 4$ Å, the number of variables in such a study is close to, and probably exceeds, the number of independent data points. Fits such as these are probably better thought of as simulations of the data—i.e. as representing one (perhaps of many) possible structural models for the data.

3.2. What is the structure in solution (de novo determination)?

Structural characterization of a structurally unknown solute is probably the most common application of XAS, especially in the context of coordination chemistry. Conceptually, the problem is straightforward; one measures the XAS spectra for one or more of the atoms in the solute and uses this information to determine the

structure of the solute. In practice, the situation can be substantially more complicated because of the limitations in the information content of XAS. Recent XAS studies of organocuprates illustrate the applications, and some of the difficulties, of XAS as a probe of solution structure.

Organo-, cyano-cuprates are the reagents formed from the addition of alkyl groups to CuCN. Although these are extremely useful reagents in organic chemistry, their structures are not well characterized. In particular, the nature of the reagent formed from adding two equivalents of alkyllithium to CuCN has been controversial. This reagent shows unique reactivity patterns. NMR spectra have been interpreted as providing evidence either for [27] or against [28] the presence of a so-called 'higher order' cyanocuprate complex. The latter would contain a three-coordinate Cu(I), with the cyanide and both of the alkyl groups coordinated to the Cu.

This is a straightforward question to answer using XAS [29]. The FTs of the EXAFS spectra for CuCN·2LiCl + *n*BuLi are shown in Fig. 7. In this case, even qualitative examination is sufficient to answer the major structural questions. The salt CuCN is not by itself soluble in THF, however it can be solubilized by addition of LiCl. The peak at approximately 3 Å in the FT for CuCN·2LiCl (Fig. 7) is due to Cu–C–N multiple scattering. The multiple scattering is intense due to the linearity of the cyanide group. This spectrum thus clearly shows that the cyanide ligands remain coordinated to the Cu in CuCN·2LiCl. The additional strong peak at about 4.5 Å can only arise from Cu–C–N–Cu multiple scattering, since there is

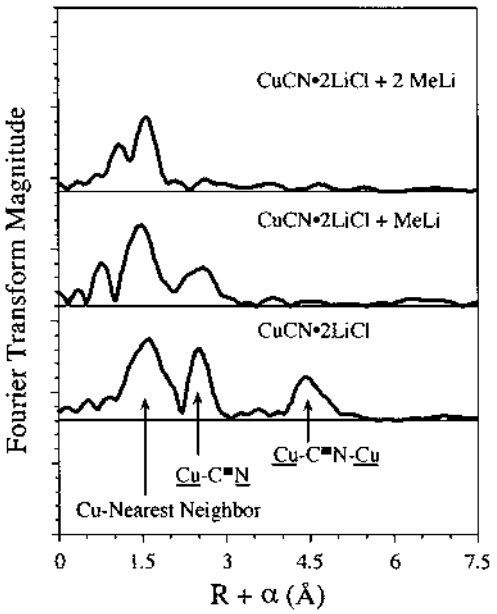

Fig. 7. Fourier transforms of the EXAFS data for CuCN·2LiCl + *n*BuLi ($n = 0, 1, 2$). Redrawn from data in Ref. [29]. All spectra measured at 10 K. See text for interpretation of these data.

nothing else in solution that can give rise to a strong scattering peak at this distance. This indicates that the CuCN is present as oligomers under these conditions. On addition of one equivalent of BuLi the Cu···Cu interaction disappears, showing that the oligomeric structure is disrupted, and the amplitude of the Cu···N interaction decreases. The latter suggests that some of the cyanide groups have been displaced, presumably by butyl ligands. On addition of the second equivalent of BuLi, all of the outer-shell interactions disappear. This is consistent with formation of Bu_2Cu^-, and inconsistent with the presence of a linear cyanide group in the putative higher-order cuprate $Bu_2Cu(CN)^{2-}$.

It is important to note that qualitative examination of Fig. 7 does not, by itself, prove that cyanide is not coordinated to Cu in CuCN·2LiCl + 2BuLi, but only that cyanide is not coordinated in the linear fashion found in $BuCuCN^-$ and CuCN·2LiCl. A hypothetical side-bound cyanide [30] could also account for the absence of the 3 Å peak for CuCN·2LiCl + 2BuLi. Although this kind of cyanide π-bonding is unknown in Cu(I) chemistry, it cannot be excluded by Fig. 7. However, quantitative analysis of the EXAFS data shows that both CuCN·2LiCl + BuLi and CuCN·2LiCl + 2BuLi contain two-coordinate Cu, as judged either by the EXAFS amplitude or by the Cu–C bond length [29]. In addition, the XANES data for CuCN·2LiCl + 2BuLi and for an authentic π-bound cuprate–alkene complex are dramatically different [31].

Several lessons can be taken from these data. One concerns the utility of multiple scattering. In these data, the only significant multiple scattering arises from the linear cyanide. This means that the multiple scattering is intense and that only a few parameters are necessary to describe it. Under these conditions, it was possible to define the Cu–C–N and Cu···N–Cu angles, both of which must have average values of 180° in order to explain the relative distances and the large amplitude of the outer shell scattering. Even with linear Cu–C–N–Cu groups, however, the ability to detect EXAFS at such long distances is due in part to the fact all of the measurements were made at 10 K, where thermal motion is minimized.

A more subtle lesson regards the availability of systematic chemical perturbations. The FT for CuCN·2LiCl + 2BuLi alone does not provide as convincing a structural picture as is provided by comparing the effect of successive BuLi additions. In general, EXAFS is more useful for relative structure comparisons (with respect to a solid state reference or between different solution structures) than as an isolated experiment.

Finally, it is important to note what was not determined in this study. The detailed geometry of the CuCN aggregate in CuCN·2LiCl cannot be defined from this work. It is, in fact, not even possible to say from the EXAFS data what role the Cl^- plays in solubilizing the CuCN. There is a small shoulder at $R + \alpha \approx 2$ Å that might be due to a Cu–Cl interaction, but based on quantitative curve fitting, it was not possible to show that Cl was required to model the EXAFS. In order to demonstrate that this shoulder does arise from Cl, it was necessary to make the LiBr substituted analog and show, using both Cu and Br EXAFS, that there is a Cu–halide interaction (data not shown). It is also important to note that the EXAFS data do not demonstrate directly that CuCN·2LiCl + BuLi contains

$BuCuCN^-$ rather than a 50:50 mixture of $Cu(CN)_2^-$ and Bu_2Cu^-, since these would have equivalent average structures. Chemical logic, together with the sequential effects of BuLi addition, dictate that it is $BuCuCN^-$ that is formed, but solution speciation cannot be shown by a single EXAFS spectrum alone (although see below for other approaches to the speciation problem). Finally, with regard to the original question of what structural properties account for the unique reactivity of $CuCN{\cdot}2LiCl + 2RLi$, it is important to note that the data in Fig. 7 do not rule out the possibility that there is a small amount of $Bu_2Cu(CN)^{2-}$ present in solution. EXAFS only provides information about the bulk solution structure. This cannot address reactivity questions, since even a minor component could be responsible for the reactivity. EXAFS is sufficient, however, to distinguish between the different interpretations of the NMR data, since EXAFS and NMR both give bulk structure.

3.3. What is the structure in the crystal (use of XAS to resolve crystallographic disorder)?

The examples used thus far involve applications of XAS to non-crystalline systems. However, XAS is also important for characterizing the structure of metal ions in crystals. This is because of the fact that crystallographic structure determination can suffer from resolution limitations analogous to those in EXAFS. In particular, the crystallographically determined structure for a metal ion that occupies a high symmetry site in a crystalline lattice is necessarily high symmetry. However, the structure of a single one of these metal sites may in fact have much lower symmetry. In such cases both X-ray diffraction, which gives the structure averaged over all unit cells, and XAS, which gives the structure averaged over all metal sites, are necessary for a complete description of the structure.

A good example of this is provided by Cu(II), which is expected to undergo a Jahn–Teller distortion to give an orbitally non-degenerate distorted structure, but which occasionally crystallizes in a high-symmetry lattice, inconsistent with such a distortion. For example, the tripodal ligand tris(2-pyridyl)methane gives a Cu(II) complex that crystallizes in $R\bar{3}$ with $\bar{3}$ Cu site symmetry. This gives six identical Cu–N bond lengths of 2.10 Å, in apparent violation of the Jahn–Teller theorem. EXAFS studies [32] showed that the Cu site in bis[tris(2-pyridyl)methane]Cu(II) nitrate has the expected tetragonal distortion, with four short (2.04 Å) and two long (2.25 Å) Cu–N distances. The apparent discrepancy between the EXAFS and the crystallographic structures can be resolved by recognizing that the orientation of the tetragonal elongation is disordered over the three different Cu–N directions. Consistent with this, the average Cu–N distances determined by EXAFS and crystallography are the same.

An important lesson in this study is that crystallographic parameters alone may not provide evidence for the presence of problems in the crystallographic refinement. A few of the ligand dimensions in the crystal structure of bis[tris(2-pyridyl)methane]Cu(II) nitrate showed significant ($\geq 3\sigma$) changes between 295 and

173 K. However, in the absence of the EXAFS data, these might have been explained as due simply to an underestimate of the uncertainty. Moreover, variable temperature X-ray diffraction is not routinely used in studies of coordination complexes, thus in many crystal structures, even this anomaly would not have been noted. The thermal parameters for the Cu and N atoms in bis[tris(2-pyridyl)methane]Cu(II) nitrate do not show particular evidence for the underlying crystallographic disorder. Without the use of both EXAFS and crystallography, it would have been difficult or impossible to obtain a complete description of the structure.

There are, of course, techniques other than EXAFS that could have indicated that the Cu did not have $\bar{3}$ symmetry. EPR, for example, is very useful in this regard. However, EPR is not as structurally definitive. For example, crystallography indicated that the $CuCl_6^{4-}$ ion in (3-chloroanilinium)$_8$($CuCl_6$)Cl_4 had an unusual tetragonally compressed structure, with two short (2.28 Å) and four long (2.61 Å) Cu–Cl bond lengths, and the EPR spectra were interpreted as being consistent with this structure [33]. In contrast, EXAFS shows that the Cu site has a more conventional elongated structure, with two pairs of short Cu–Cl bond lengths (2.28 and 2.38 Å) and one pair of long Cu–Cl bond lengths (2.83 Å) [34]. In this case, the long Cu–Cl distance and the longer of the two short Cu–Cl distances are crystallographically disordered.

3.4. How does the structure evolve with time?

An exciting new development in XAS is the ability to measure time resolved spectra with a time resolution that extends, in principal, into the microsecond regime. This means that XAS can be used to determine the kinetics of a reaction. For many reactions, this is not particularly useful, since it may be substantially easier to measure reaction kinetics using more conventional spectroscopies. There are, however, two important areas in which time-resolved XAS can provide unique information. The first is for spectroscopically 'silent' metals that do not have other available spectroscopic signatures. Examples include Cu(I) and Zn(II). In these cases, XAS may provide the only direct probe of the time dependence of the structure. The importance of XAS in these cases is as a tool for measuring rate constants.

A second area where XAS can contribute to kinetic studies is in the characterization of reactive intermediates. Reactive intermediates are, by definition, difficult or impossible to crystallize. They may, however, be accessible to structural characterization using XAS. The difficulty, as noted earlier, is that bulk techniques such as XAS cannot easily be used to measure structure for minor components in a complex mixture. An elegant example of how time-resolution can be used to circumvent this limitation is provided by a recent study of a vanadium oxidation catalyst [35]. In this case, hundreds of XAS spectra were measured with 1 s time resolution as the reaction (oxidation of *n*-butane over a vanadium phosphate catalyst) took place. No single spectrum gave sufficient information that could be

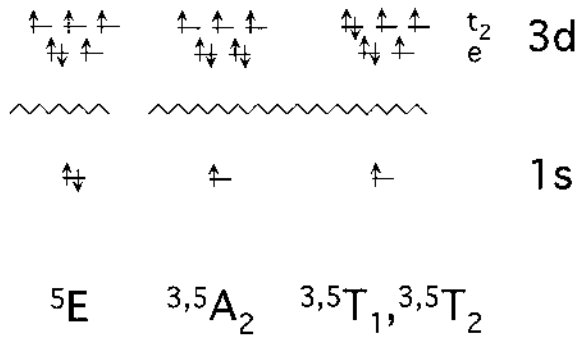

Fig. 8. Schematic illustration of the transitions involved in the $1s \rightarrow 3d$ region for a tetrahedral Fe(II) site. Ground state is shown on the left, the two possible 1-electron excited configurations are shown on the right. See Ref. [39] for detailed description of multiplet interpretations of $1s \rightarrow 3d$ data.

used to distinguish the different species that were present. However, by using principal component analysis, it was possible to identify contributions from three different species (one present at ca. 20 mol%) that contributed to the overall data variation. From comparison with standards these components could be assigned to V^{5+}, V^{4+}, and V^{3+}.

In this case, the ability to identify and characterize minor components rests on the addition of a new dimension (i.e. time) to the data. Another way to increase the information content of XAS is to add spatial, rather than temporal, resolution. With modern synchrotron facilities it is now possible to record XAS spectra from 1×1 μm square samples [36,37]. To date, this has largely been used by the geological community to prepare maps of species distributions in complex samples (e.g. [38]). However, this could also be used, for example, to examine the products of combinatorial inorganic reactions in order to characterize, for example, the most promising catalyst.

3.5. What is the electronic structure of the metal?

Thus far, reference has been made to the XANES region only as providing a fingerprint for different structural environments. However, the bound-state transitions (e.g. $1s \rightarrow 3d$, $1s \rightarrow 4p$ for the first transition series metals) can be analyzed to obtain direct insight into the electronic structure of the absorbing atom. For example, Solomon and co-workers have recently used Fe XANES spectra to characterize the electronic environment of Fe(II) and Fe(III) sites [39]. For tetrahedral Fe(II), there are two possible one-electron excited states that correspond to '$1s \rightarrow 3d$' transitions, as shown in Fig. 8. The $(e)^4(t_2)^3$ configuration gives rise to a $^4A_2$ many-electron state, while the $(e)^3(t_2)^4$ configuration gives rise to $^4T_1$ and $^4T_2$ many-electron states. In addition, a two-electron configuration $(e)^2(t_2)^5$ also gives a $^4T_1$ state that will mix with the lower energy $^4T_1$ state. These quartet states couple

to the half-occupied 1s level to give triplet and quintet states, with only the latter giving observable transitions. The energies of the different many-electron states were estimated using Tanabe–Sugano matrices. All of these transitions are weak (see, for example, the low intensity of the $1s \rightarrow 3d$ transition in Fig. 1) because a pure $1s \rightarrow 3d$ transition is forbidden by dipole selection rules. Although the $1s \rightarrow 3d$ transitions are allowed by quadrupole selection rules [40], the major source of intensity is mixing of the metal 4p into the 3d states. For the Fe(II) and Fe(III) complexes, the intensities of the different transitions were evaluated using density functional theory to calculate the amount of 4p character that is mixed into each of the excited states. This type of analysis holds a great deal of promise for allowing XANES to be used to extract detailed electronic information about the absorbing atom.

An alternative, complementary, approach to electronic structure information is to use ligand XANES rather than metal-site XANES spectra. This is particularly promising as a tool for investigating sulfur or chlorine ligands [41,42] and has been used to quantitate the amount of metal–ligand orbital mixing (i.e. the covalency) of different complexes. For example, excitation at the Cl K edge gives rise to an allowed $1s \rightarrow 3p$ transition. Since the Cl 3p orbitals are the bonding orbitals, the lowest energy transition at the Cl edge is actually a $1s(Cl) \rightarrow HOMO$ transition, where the HOMO has both metal 3d and Cl 3p character. The intensity of this transition is a direct measure of the percent 3p character of this orbital (i.e. the covalency of the complex).

The increased sensitivity of ligand XANES (as compared to metal XANES) for electronic structure determination is due in part to the fact that the transitions of interest from a bonding perspective are $1s \rightarrow 3p$ for S or Cl ligands and $1s \rightarrow 3d$ for a metal from the first transition series. The former is an allowed transition while the latter is forbidden, and consequently much weaker and harder to detect. An alternative is to use the 2p initial state of the metal (i.e. the L edge) to study transition metal electronic structure. This has been used to good effect for second transition series metals, but requires experimentally difficult (i.e. vacuum UV) energies for the first transition series metals.

Two recent developments in experimental methodology bear comment in the context of electronic structure determination. The first involves the use of high-resolution X-ray emission rather than X-ray absorption to probe electronic structure. In principle, the information content is complementary, since X-ray emission probes the filled electronic levels, while X-ray absorption probes the empty levels. In practice, X-ray fluorescence is often able to provide much better energy resolution than is obtained by X-ray absorption [43,44]. The second, which is particularly important for magnetic sites, involves taking advantage of the differential absorption of left and right circularly polarized X-rays in a magnetically oriented sample [45]. This is the X-ray analog of magnetic circular dichroism. In studies of model systems, X-ray MCD seems able to provide even more detailed information than can be obtained from conventional XAS.

4. Prospects for the future

Given the potential range of applications of XAS in coordination chemistry, it is worth asking why the method has not received greater attention. One obvious factor involves the difficulty of making XAS measurements. All of the spectra discussed in this paper were measured at synchrotron radiation facilities. Until recently, it was extremely difficult to get access to the limited beam time available at these facilities, and to some extent this may still limit the applications of XAS. In addition, the need to travel to a distant laboratory in order to make measurements represents a powerful social force limiting wider application of XAS. Both of these are changing, as the amount and quality of synchrotron beam time has increased, and as the scientific community has become more accustomed to using large specialized facilities to make measurements. It is important to note that some of the methods that were discussed, for example time resolved measurements, high-resolution X-ray fluorescence and X-ray MCD are very new, and depend on the capabilities of the newest synchrotron sources. As time advances, these are likely to become both more accessible and more widely appreciated. This is reflected in the increasing number of 'non-XAS' papers which make use of XAS as one of the tools for characterizing coordination complexes (including many papers which have not been mentioned here). There is every reason to believe that this trend will continue, and that XAS will become one of the standard tools used to characterize coordination compounds.

Acknowledgements

I gratefully acknowledge support of our XAS studies by the NIH (Grants GM-38047 and GM-45205) and of the US synchrotron sources by the US Department of Energy. The measurements discussed in this tutorial were made at the Stanford Synchrotron Radiation Laboratory and the National Synchrotron Light Source. Finally, I thank Bill Rutherford and his group for support and hospitality during a sabbatical stay in Saclay.

References

[1] S.P. Cramer, Chem. Anal. 92 (1988) 257.
[2] R.A. Scott, Methods Enzymol. 117 (1985) 414.
[3] C.D. Garner, in: C.R.A. Catlow, G.N. Greaves, X-ray absorption spectroscopy of biological molecules, Blackie, Glasgow, 1990, p. 268.
[4] D.C. Koningsberger, R. Prins (Eds.), X-ray Absorption: Principles, Applications, Techniques of EXAFS, SEXAFS, and XANES, Wiley, New York, 1988.
[5] P.A. Lee, P.H. Citrin, P. Eisenberger, B.M. Kincaid, Rev. Mod. Phys. 53 (1981) 769.
[6] E.D. Crozier, Nucl. Instrum. Methods Phys. Res. B 133 (1997) 134.
[7] B.K. Teo, EXAFS: Basic Principles and Data Analysis, Springer, New York, 1986.
[8] P.J. Riggs-Gelasco, T.L. Stemmler, J.E. Penner-Hahn, Coord. Chem. Rev. 144 (1995) 245.

[9] M. Vaarkamp, I. Dring, R.J. Oldman, E.A. Stern, D.C. Koningsberger, Phys. Rev. B 50 (1994) 7872.
[10] J.J. Rehr, D.L.J. Mustre, S.I. Zabinsky, R.C. Albers, J. Am. Chem. Soc. 113 (1991) 5135.
[11] J.J. Rehr, R.C. Albers, S.I. Zabinsky, Phys. Rev. Lett. 69 (1992) 3397.
[12] K. Clark-Baldwin, D.L. Tierney, N. Govindaswamy, E.S. Gruff, C. Kim, J. Berg, S.A. Koch, J.E. Penner-Hahn, J. Am. Chem. Soc. 120 (1998) 8401.
[13] P.J. Riggs-Gelasco, R. Mei, C.F. Yocum, J.E. Penner-Hahn, J. Am. Chem. Soc. 118 (1996) 2387.
[14] E.A. Stern, Phys. Rev. B 48 (1993) 9825.
[15] A. Michalowicz, G. Vlaic, J. Synchron. Rad. 5 (1998) 1317.
[16] S. Wang, M.H. Lee, R.P. Hausinger, P.A. Clark, D.E. Wilcox, R.A. Scott, Inorg. Chem. 33 (1994) 1589.
[17] R.W. Strange, N.J. Blackburn, P.F. Knowles, S.S. Hasnain, J. Am. Chem. Soc. 109 (1987) 7157.
[18] R.W. Joyner, K.J. Martin, P. Meehan, J. Phys. C: Solid State Phys. 20 (1987) 4005.
[19] G. Bunker, S. Hasnain, D. Sayers, in: S.S. Hasnain (Ed.), X-ray Absorption Fine Structure, Ellis Horwood, New York, 1991, p. 751.
[20] F.W. Lytle, D.E. Sayers, E.A. Stern, Physica B 158 (1988) 701.
[21] M.S. Lah, B.R. Gibney, D.L. Tierney, J.E. Penner-Hahn, V.L. Pecoraro, J. Am. Chem. Soc. 115 (1993) 5857.
[22] J.E. Penner-Hahn, M. Murata, K.O. Hodgson, H.C. Freeman, Inorg. Chem. 28 (1989) 1826.
[23] R.A. Scott, J.E. Hahn, S. Doniach, H.C. Freeman, K.O. Hodgson, J. Am. Chem. Soc. 104 (1982) 5364.
[24] M.D. Wirt, L. Bubacco, J. Peisach, Inorg. Chem. 34 (1995) 2377.
[25] P. D'Angelo, E. Bottari, M.R. Festa, H.-F. Nolting, N.V. Pavel, J. Phys. Chem. B 102 (1998) 3114.
[26] P. D'Angelo, E. Bottari, M.R. Festa, H.-F. Nolting, N.V. Pavel, J. Chem. Phys. 107 (1997) 2807.
[27] B.H. Lipshutz, S. Sharma, E.L. Ellsworth, J. Am. Chem. Soc. 112 (1990) 4032.
[28] S.H. Bertz, J. Am. Chem. Soc. 112 (1990) 4031.
[29] T.L. Stemmler, T. Barnhart, J.E. Penner-Hahn, C.E. Tucker, P. Knochel, M. Böhme, G. Frenking, J. Am. Chem. Soc. 117 (1995) 12489.
[30] B.H. Lipshutz, B. James, J. Org. Chem. 59 (1994) 7585.
[31] T.M. Barnhart, H. Huang, J.E. Penner-Hahn, J. Org. Chem. 60 (1995) 4310.
[32] T. Astkey, P.J. Ellis, H.C. Freeman, M.A. Hitchman, F.R. Keene, E.R.T. Tiekink, J. Chem. Soc. Dalton Trans. (1995) 595.
[33] D. Tucker, P.S. White, K.L. Trojan, M.L. Kirk, W.E. Hatfield, Inorg. Chem. 30 (1991) 823.
[34] P.J. Ellis, H.C. Freeman, M.A. Hitchman, D. Reinen, B. Wagner, Inorg. Chem. 33 (1994) 1249.
[35] G.W. Coulston, S.R. Bare, H. Kung, K. Birkeland, G.K. Bethke, R. Harlow, N. Nerron, P.L. Lee, Science 275 (1997) 191.
[36] S.R. Sutton, M.L. Rivers, S. Bajt, K. Jones, J.V. Smith, Nucl. Instrum. Methods Phys. Res. Sect. A 347 (1994) 412.
[37] R.S. Sutton, S. Bajt, J. Delaney, D. Schulze, T. Tokunaga, Rev. Sci. Instrum. 66 (1995) 1464.
[38] P.M. Bertsch, D.B. Hunter, S.R. Sutton, S. Bajt, M.L. Rivers, Environ. Sci. Technol. 28 (1994) 980.
[39] T.E. Westre, P. Kennepohl, J.G. DeWitt, B. Hedman, K.O. Hodgson, E.I. Solomon, J. Am. Chem. Soc. 119 (1997) 6297.
[40] J.E. Hahn, R.A. Scott, K.O. Hodgson, S. Doniach, S.R. Desjardins, E.I. Solomon, Chem. Phys. Lett. 88 (1982) 595.
[41] I.J. Pickering, G.N. George, Inorg. Chem. 34 (1995) 3142.
[42] S.E. Shadle, B. Hedman, K.O. Hodgson, E.I. Solomon, J. Am. Chem. Soc. 117 (1995) 2259.
[43] K. Hamalainen, C.C. Kao, J.B. Hastings, D.P. Siddons, L.E. Berman, V. Stojanoff, S.P. Cramer, Phys. Rev. B: Condens. Matter 46 (1992) 14274.
[44] K. Hamalainen, D.P. Siddons, J.B. Hastings, L.E. Berman, Phys. Rev. Lett. 67 (1991) 2850.
[45] J. van Elp, S.J. George, J. Chen, G. Peng, C.T. Chen, L.H. Tjeng, G. Meigs, H.J. Lin, Z.H. Zhou, M.W.W. Adams, B.G. Searle, S.P. Cramer, Proc. Natl. Acad. Sci. USA 90 (1993) 9664.